Dense Estimation of Surface Reflectance Parameters by Selecting Optimum Illumination Conditions

Takashi Machida, Haruo Takemura* and Naokazu Yokoya
Graduate School of Information Science, Nara Institute of Science and Technology
8916-5 Takayama, Ikoma, Nara 630-0101, Japan
E-mail: {taka-ma, takemura, yokoya}@is.aist-nara.ac.jp

Abstract

To reproduce a real object in CG, a texture method which uses a real image has been widely investigated. In this method, when the object is represented as a virtual object, the object sometimes looks unnatural since the real image is influenced by a real illumination condition. Thus, it is necessary to estimate reflectance properties of object surfaces. Some researchers have been attempted to solve this problem using range and texture images. However, since the specular reflection component which is one of the surface reflectance properties cannot always be observed, an assumption with a shape and a surface property of the object is needed. This paper describes a new method of densely estimating non-uniform surface reflectance properties of real objects with convex and concave surfaces using registered range and surface color texture images obtained by a laser rangefinder. The proposed method determines positions of light to take color images for discriminating diffuse and specular reflection components of surface reflection. The Torrance-Sparrow model is employed to estimate reflectance parameters by using color images under multiple illumination conditions. Experiments show the usefulness of the proposed method.

1 Introduction

Image based rendering (IBR) methods often have been used to reproduce real objects in computer graphics (CG). Since a real image of an object is used as a texture of the object in IBR, a problem occurs, i.e., the appearance of the object is not reproduced appropriately when lighting conditions of real and CG environments are not consistent.

To overcome the problem, a number of methods of estimating reflectance properties of an object surface have been developed [1, 3, 4, 5, 6, 7, 8]. In these methods, reflection models with several parameters are employed and shape and color information of the object is used to estimate the reflectance parameters.

In some works [1, 3, 7], it is assumed that an object has uniform reflectance properties over the entire surface. Reflectance parameters are estimated by using the standard least-squares method with a color image. Due to the assumption, these methods cannot be applied to objects which consist of several different materials and have non-uniform reflectance properties. To treat non-uniform surface objects, Kay and Caelli [4] have proposed a method which uses multiple images of an object under different lighting conditions and estimates reflectance parameters by solving simultaneous equations. However, the method still has a problem that results are not stable especially when the specular reflection component, which is one of the reflection component, is very small.

Recently, Sato et al. [8] have developed a methodology to estimate non-uniform reflectance properties. They set up an object on a robot arm and measure the object with a CCD camera and a rangefinder from a large number of viewpoints by rotating the robot arm. In the method, reflectance parameters are stably acquired by decomposing the surface reflection into two components based on the singular value decomposition (SVD) technique. Although the method can be applied to objects with non-uniform reflectance properties, the shape of an object should be limited to convex. This is because it is difficult to observe the specular reflection component over the surface, since the lighting condition for a pose of the object against the camera cannot be changed in the method.

We propose a new method for estimating non-uniform reflectance properties by observing the specular reflection component densely in the image obtained by a laser rangefinder which accurately takes registered range and color images of an object. In this paper, an algorithm is proposed to determine light positions with which the specular reflection component is strongly observed over the surface of a complex object with convex and concave surfaces.

*Presently with Cybermedia Center, Osaka University.

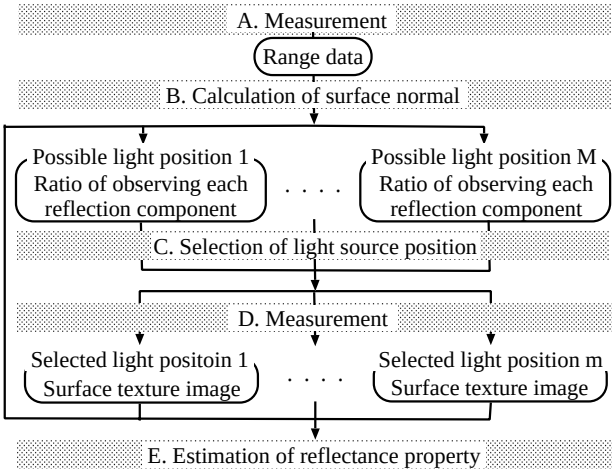

Figure 1. Flow diagram of estimating surface reflectance properties.

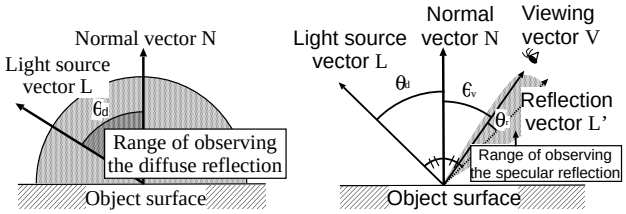

(a) Diffuse reflection (b)Specular reflection

Figure 2. Diffuse and Specular reflection on an object surface.

2 Estimation of reflectance parameters from range and color images

2.1 Overview

In the present work, the Torrance-Sparrow model is employed as a surface reflectance model to estimate object surface reflectance properties from range and color images. Figure 1 shows a flow diagram of estimating surface reflectance properties. Our process consists of four parts, which are a measurement of an object (A, D), a preprocessing (B), a selection of light source (C), and an estimation of reflectance property (E).

2.2 Torrance-Sparrow model

In this paper, the Torrance-Sparrow model [9], which accurately represents object reflectance properties, is employed to estimate reflectance parameters. The Torrance-Sparrow model is given as:

$$i = \frac{1}{C^2}(i_d + i_s), \quad (1)$$

$$i_d = P_d(\mathbf{N} \cdot \mathbf{L}), \quad (2)$$

$$i_s = \frac{P_s}{(\mathbf{N} \cdot \mathbf{V})} exp(-\frac{(cos^{-1}(\mathbf{V} \cdot \mathbf{L}'))^2}{2\sigma^2}), \quad (3)$$

$$\mathbf{L}' = 2(\mathbf{N} \cdot \mathbf{L})\mathbf{N} - \mathbf{L}, \quad (4)$$

where i represents an observed intensity, i_d and i_s denote the diffuse and specular reflection components, C is an attenuation efficient concerning the distance between a point light source and an object surface point, P_d is the diffuse reflectance parameter, P_s is the specular reflectance parameter, σ is the surface roughness parameter which is the standard deviation of a Gaussian distribution, $\mathbf{L}$ is a light source vector, $\mathbf{N}$ is a surface normal, $\mathbf{V}$ is a viewing vector, and $\mathbf{L}'$ is a reflection vector which is $\mathbf{L}$ mirrored against $\mathbf{N}$ and is given by Equation (4), respectively. All vectors are unit vectors. Figure 2 illustrates the geometry for this model.

In the case of color image, i, i_d, i_s, P_d and P_s consist of RGB channels and this model is applied to each channel. In order to estimate reflectance parameters P_d, P_s and σ, it is necessary to obtain the other parameters i, C, $\mathbf{L}$, $\mathbf{V}$ and $\mathbf{N}$ at each point of the object surface.

2.3 Measurement of an object

To obtain unknown parameters other than reflectance parameters in the Torrance-Sparrow model, we use a laser rangefinder (Cyberware 3030RGB) with known positions of point light sources and a camera for acquiring surface color images, as illustrated in Figure 3(a). Figure 3(b) shows its motion during measurement and Figure 3(c) shows the illustration viewed from the top of the device. This system can obtain registered range and surface color texture images at the same time by rotating the rangefinder and the camera around an object, so that there is no registration error, even when an object is measured many times. By using accurately registered multiple color images, reflectance parameters can be estimated accurately by solving simultaneous equations. In Figure 3(c), a camera is located at $X1$ and a texture image is acquired through mirrors which are located at $X2$ and $X3$. We assume that the camera is located at $X4$ virtually and the camera looks toward the center of rotation.

2.4 Preprocessing

Generally, the noise and quantization error are included in the range image acquired from the laser rangefinder. There is also a problem that the surface normal is not calculated accurately around the discontinuity in the range image. Therefore, we employ local quadratic surface fitting.

Firstly, the 5×5 median filter is applied to the range image to remove the noise. Secondly, the quadratic surface is locally fitted with the range image. The range image is expressed by the cylindrical coordinates. Each point of the

(a) Appearance of 3D-Digitizer

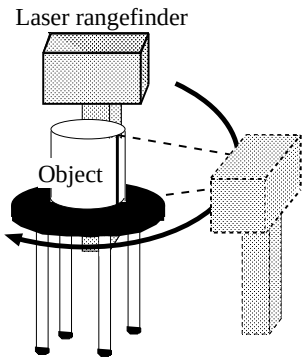

(b) Motion during measurement

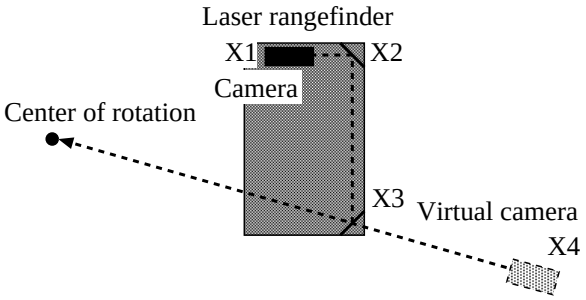

(c) Direction of camera

Figure 3. 3D-Digitizer.

range image is represented as:

$$\begin{aligned}(x, y, z) &= \{-r(s,t)\sin(s), -t, -r(s,t)\cos(s)\} \\ &= \mathbf{S}(s,t), \end{aligned} \quad (5)$$

where r, s, t are the distance from the center of rotation, the angle of rotation, and the height along the rotation axis, respectively.

The unit normal vector is given as follows:

$$\begin{aligned}\mathbf{N} &= \frac{\mathbf{S}_s \times \mathbf{S}_t}{\|\mathbf{S}_s \times \mathbf{S}_t\|} \quad (6) \\ &= \frac{1}{\sqrt{r_s^2 + r^2 + r^2 r_t^2}}\{-r_s\sin(s) - r\cos(s), \\ &\qquad -r_t r, \\ &\qquad -r_s\cos(s) + r\sin(s)\},\end{aligned}$$

where r_s, r_t are gradient components of the range image $r(s,t)$. This gradient is computed using the following local surface fit:

$$r'(s,t) = as^2 + bt^2 + cst + ds + et + f, \quad (7)$$

$$r'_s = 2as + ct + d, \quad (8)$$

$$r'_t = 2bt + cs + e. \quad (9)$$

Coefficients $a \sim f$ are determined by minimizing the following equation using the range data $r(s,t)$ and Equation (7).

$$\begin{aligned}error(s,t) &= \sum_{u=-2}^{2}\sum_{v=-2}^{2}\{r(s+u,t+v) \\ &\qquad -r'(s+u,t+v)\}^2, \quad (10)\end{aligned}$$

where u, v are local coordinates in a 5×5 window. In our approach, selected local quadratic surface fit is achieved by using the Yokoya-Levine operator [10]. In [10], the best window is selected among 25 windows which include the point (s,t) to estimate the coefficients $a \sim f$ at (s,t). The best window provides the minimum fitting error in Equation (10). Then, r'_s and r'_t are computed from Equation (8), (9) and the estimated coefficients $a \sim f$.

2.5 Selection of light source

It is important to observe the strong specular reflection component to make calculations stable, since the specular reflection component is observed only within a limited range of angle around the reflection vector. Illumination conditions must be changed according to the shape of measured object. To achieve this, multiple positions of a light are determined among M possible positions prepared around the laser rangefinder as shown in Figure 4. The light source rotates with the laser rangefinder. The number of possible positions is 60 $(M = 60)$ in the present setup and these are arranged with 5 vertically and with 12 horizontally at the interval of 5 cm. The positions of a light source and a camera are calibrated by measuring a box whose size is known. When multiple possible positions are selected, a single light is attached at selected possible positions in turn. Therefore, the calibration of brightness among multiple lights is not needed. With respect to the change of brightness of the light source by the distance between the object and the light source, it is considered as the attenuation of the light source by Equation (1).

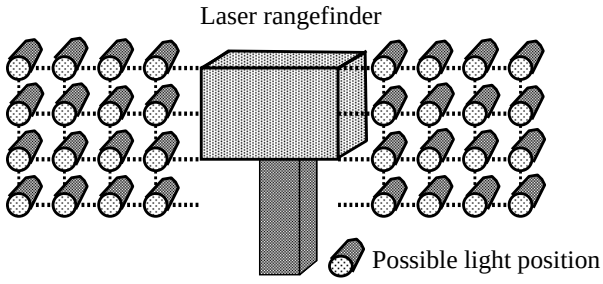

Figure 4. Multiple possible light source positions.

To densely estimate non-uniform reflectance parameters independently, it is needed to observe the two reflection components separately for each pixel. However, since the diffuse reflection component is observed over the object surface, it is impossible to observe only the specular reflection component. The specular reflection component can be calculated by subtracting a value of a pixel which includes only the diffuse reflection component from that of the pixel which includes both the diffuse and specular reflection components. Therefore, it is needed to observe a pixel under three different lighting conditions: One for observing only the diffuse reflection component to acquire one unknown parameter P_d based on Equation (2) and others for observing both the diffuse and specular reflection components to acquire two unknown parameters P_s and σ by solving simultaneous equations based on Equation (3). To observe every pixel under appropriate three different lighting conditions, the positions of the light are selected from M possible positions.

Let I_p be a color image which is to be obtained with a possible light position p $(p = 1, \cdots, M)$ and consists of n pixels $(i_{p1}, \cdots, i_{pn})$, where i_{pk} means a color intensity, D_p be the number of pixels which include only the diffuse reflection component in I_p, and S_p be the number of pixels which include the specular reflection component strongly in I_p.

First, the following items are judged for each pixel in the object surface texture under each light position p.

- **Measurability of the light reflection**
- **Measurability of only the diffuse reflection**
- **Measurability of the strong specular reflection**

Second, the light positions p and q which satisfy $D_p = Max(D_1, \cdots, D_M)$ and $S_q = Max(S_1, \cdots, S_M)$ are selected. In the next light source position selection, the position which satisfies the same condition is selected among the rest except for light source positions decided so far. Then, m light positions are selected to densely estimate reflectance parameters. The selections of positions are repeated until almost all pixels are observed once for only the diffuse reflection component and twice for the strong specular reflection component.

We introduce a threshold th, i.e., the ratio of the measurability of both reflection components to stop the process of selecting light positions. With respect to determining the threshold th, we judge the ratio of the measurability of the specular reflection with all possible positions. This ratio is a limit of measuring the specular reflection component. Using the threshold, we can terminate the light selection process in the case that even if the number of positions of light source is increased, the ratio of measurability of specular reflection component cannot increase more. Therefore, reflectance parameters can be efficiently estimated almost the whole object surface using a limited number of texture images.

2.5.1 Measurability of the light reflection

In order to measure the light reflection at a specific point of the object surface, the point on the surface must be observable from the camera position. Additionally positional relationship among the camera, the point and the light source must satisfy the following conditions.

$$(\mathbf{V}_k \cdot \mathbf{N}_k) > \mathbf{0}, \ (\mathbf{L}_{pk} \cdot \mathbf{N}_k) > \mathbf{0}, \tag{11}$$

where $\mathbf{V}_k$, $\mathbf{L}_{pk}$, and $\mathbf{N}_k$ are the viewing direction, the light source direction, and the surface normal at the k-th pixel, respectively. Note that the viewing direction $\mathbf{V}_k$ and the surface normal $\mathbf{N}_k$ are independent of the light source position p.

Even when the above equations are both satisfied, there is a possibility that a shadow is casted on the pixel. Figure 5 shows such a case. In this case, the pixel must not be used for estimating reflectance parameters. Whether a point o is covered by a shadow casted by light source p or not can be judged as follows.

Let $(x, y, z) = (o_x, o_y, o_z)$ be the coordinates of the point o on the object surface, $(x, y, z) = (p_x, p_y, p_z)$ be the coordinates of the possible light position. There is a bounding box which is surrounded by the maximum and minimum values on each x, y, z axis of position p and o as shown in Figure 5. Here, we can assume that all polygons which make the object surface are small enough to be covered by the bounding box. Then, in order to examine if a shadow is cast over the point o, we have to examine if any polygons that contain any vertices inside the bounding box intersect with the line segment that connects o and p.

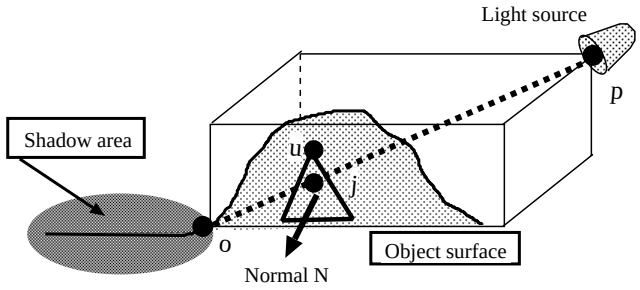

Figure 5. An illumination of detecting a self-shadow.

Therefore, for all the points inside of the bounding box, the following test is performed [2].

Let h be the point which is found to be included in the bounding box and $(x, y, z) = (h_x, h_y, h_z)$ be the coordinates of the point. If h lays on the plane whose normal vector is **N**, the plane and the line segment which links p and o are given by the following equations, respectively.

$$\begin{cases} N_x(x - h_x) + N_y(y - h_y) + N_z(z - h_z) = 0, \\ g = \dfrac{x - o_x}{p_x - o_x} = \dfrac{y - o_y}{p_y - o_y} = \dfrac{z - o_z}{p_z - o_z}. \end{cases} \tag{12}$$

The intersection of the plane and the line segment, the point j, can be obtained by solving Equation (12) about g. Now g is defined as follows.

$$\begin{aligned} g &= \frac{N_x(h_x - o_x) + N_y(h_y - o_y) + N_z(h_z - o_z)}{N_x(p_x - o_x) + N_y(p_y - o_y) + N_z(p_z - o_z)} \\ &= \frac{\mathbf{N} \cdot \mathbf{H}_o}{\mathbf{N} \cdot \mathbf{P}_o}, \end{aligned} \tag{13}$$

where $\mathbf{H}_o$ is the vector from the point h to the surface point o, $\mathbf{P}_o$ is the vector from the light position p to the surface point o. If g satisfies $0 \leq g \leq 1$ and the point j lays on the polygon which includes h, it is concluded that the line segment of Equation (12) crosses the object.

2.5.2 Measurablility of the diffuse reflection only

When the k-th pixel consists of only the diffuse reflection, the reflection vector $\mathbf{L'}_{pk}$ satisfies the following equation.

$$\theta_r = cos^{-1}(\mathbf{V}_k \cdot \mathbf{L}'_{pk}) > \theta_{th1}, \tag{14}$$

where θ_{th1} is a threshold angle between $\mathbf{V}_k$ and $\mathbf{L}'_{pk}$. Equation (14) implies that only the diffuse reflection component is observed if θ_r is greater than θ_{th1} as illustrated in Figure 6. When this condition stands and the pixel is not in a shadow, the pixel is judged to have diffuse reflection only and is counted in D_p.

2.5.3 Measurability of the strong specular reflection

When k-th pixel includes the specular reflection strongly, the reflection vector $\mathbf{L'}_{pk}$ satisfies the following equation.

$$\theta_r = cos^{-1}(\mathbf{V}_k \cdot \mathbf{L}'_{pk}) \leq \theta_{th2}, \tag{15}$$

where θ_{th2} is a threshold angle between $\mathbf{V}_k$ and $\mathbf{L}'_{pk}$. Equation (15) means that both the diffuse and specular reflection components are observed if θ_r is smaller than θ_{th2} as illustrated in Figure 7. The above condition is based on the fact that the specular reflection is observed strongly in a limited range of a viewing angle. When this condition stands and the pixel is not in a shadow, the pixel is judged to have strong specular reflection and is counted in S_p.

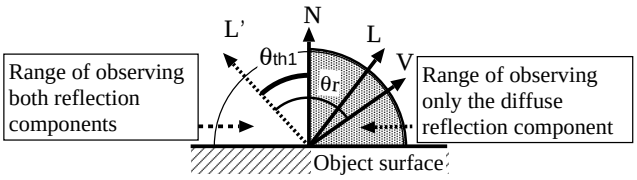

Figure 6. Observation of only the diffuse reflection component.

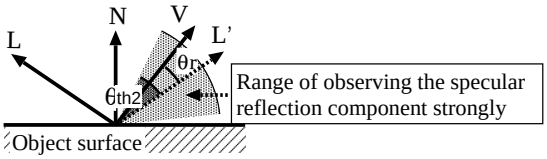

Figure 7. Observation of the specular reflection component strongly.

2.6 Estimation of reflectance parameters

After the positions of the light source are determined, multiple color images are taken under the different lighting conditions and then non-uniform reflectance parameters are estimated.

Let $I_{p,diff}$ be the set of pixels which are judged to consist of only the diffuse reflection component with possible light position p and consist of n pixels $(i_{p,diff,1}, \cdots, i_{p,diff,n})$, where $i_{p,diff,k}$ means a color intensity. Let $I_{p,both}$ be the set of pixels which are judged to include the specular reflection component strongly and consist of n pixels $(i_{p,both,1}, \cdots, i_{p,both,n})$, where $i_{p,both,k}$ means a color intensity. Note that there are some pixels which consist of neither the diffuse reflection component only, nor the strong specular reflection component in $I_{p,diff}$ and $I_{p,both}$. Let $i_{p,no,k}$ be such the k-th pixel. With respect to that pixel, reflectance parameters cannot be estimated.

2.6.1 Estimation of diffuse reflectance parameter

The diffuse reflectance parameter P_{dk} at the k-th pixel is estimated by solving Equation (2) with the value of the k-th pixel $i_{p,diff,k}$ in the image $I_{p,diff}$, $\mathbf{N}_k$ and $\mathbf{L}_{pk}$ as follows:

$$P_{dk} = \frac{C_{pk}^2 \, i_{p,diff,k}}{(\mathbf{N}_k \cdot \mathbf{L}_{pk})}. \tag{16}$$

In order to get the most reliable estimation, the pixel whose angle θ_r is the smallest but greater than θ_{th1} is selected.

2.6.2 Estimation of specular reflectance and surface roughness parameters

The specular reflectance parameter P_{sk} and the surface roughness parameter σ_k at the k-th pixel are estimated by solving Equation (3) with the value of the specular reflection component which is extracted from the k-th pixels $i_{p,both,k}$ and $i_{q,both,k}$ in the images $I_{p,both}$ and $I_{q,both}$, $\mathbf{N}_k$, $\mathbf{L}_{pk}$, and $\mathbf{V}_k$. In order to get the most reliable estimation, the pixels whose angle θ_r is the smallest or the second smallest and is smaller than θ_{th2}, are selected.

First, the diffuse reflection component is computed by substituting the estimated P_d into Equation (2). Second, the specular reflection component is extracted by subtracting the diffuse reflection component from Equation (1). Finally, the specular reflectance and surface roughness parameters are obtained by solving the following simultaneous equations that are derived from Equation (3).

$$\begin{cases} i_{m,both,k} = \frac{1}{C_{mk}^2}(i_{m,diff,k} + i_{m,spec,k}) \quad (m = p, q), \\ i_{p,spec,k} = \frac{P_{sk}}{(\mathbf{N}_k \cdot \mathbf{V}_k)} exp(-\frac{(cos^{-1}(\mathbf{V}_k \cdot \mathbf{L}'_{pk}))^2}{2\sigma_k^2}), \\ i_{q,spec,k} = \frac{P_{sk}}{(\mathbf{N}_k \cdot \mathbf{V}_k)} exp(-\frac{(cos^{-1}(\mathbf{V}_k \cdot \mathbf{L}'_{qk}))^2}{2\sigma_k^2}), \end{cases} \quad (17)$$

where $i_{p,spec,k}$ and $i_{q,spec,k}$ are specular reflection components of the pixel obtained under different two illumination conditions p and q as:

$$i_{m,spec,k} = C_{mk}^2 i_{m,both,k} - i_{m,diff,k} \quad (m = p, q), \quad (18)$$

where $i_{m,diff,k}$ is the diffuse reflection component obtained from P_{dk} estimated in the previous section, $\mathbf{N}_k$ and $\mathbf{L}_{mk}$ by using Equation (2).

It should be noted that Equation (3) cannot be solved for a pixel at which strong specular reflection is observed less than twice. In such a case, the specular reflectance and surface roughness parameters are estimated by using a linear-interpolation method within a $W \times W$ window. When the window is small against the area whose reflectance parameters are not solved, pixels are interpolated linearly by scanning the texture image horizontally.

3 Experiments

In our experiments, a measured object is a plastic doll and exibits non-uniform surface reflectance as shown in Figure 8(a) and is assumed not to have interreflections. We fix some parameters as $\theta_{th1} = 60^o$, $\theta_{th2} = 20^o$, $th = 80\%$ and the size of the window that is used to interpolate the pixel whose reflectance parameters are not estimated is 3×3 $(W = 3)$. The proposed method of selecting positions of the light source determined 12 light source positions for the object.

Figure 8(b)$\sim$ (d) show the estimated reflectance parameters coded as the color intensity in the cylindrical coordinates. Figure 8(b) illustrates the diffuse reflectance parameter estimated all over the object surface. Figure 8(c) is the specular reflectance parameters. This image shows that the specular reflectance parameter of the doll's beak and leg are different from the rest. Actually, the beak and legs are highly reflective. This result is consistent with an observation of a doll in Figure 8(a). Figure 8(d) shows the surface roughness parameter with gray-scale where the largest value is coded as white. This image means that the smaller the value is, the smoother the object surface is. Figure 8(e) shows the ratio of pixels where specular reflectance and surface roughness parameters are computed. The black part means that both parameters are not directly estimated. Non-uniform diffuse reflectance parameter was estimated on the whole observed object surface. Non-uniform specular reflectance and surface roughness parameters were estimated without interpolation for 83.46% of the surface. Note that there is a part where reflectance parameters cannot be estimated. The reason is that the normal vector is a vertical upward or downward. These parts are linearly interpolated.

Figure 9 illustrates the measurability of both reflection components with respect to the number of light sources. In these graphs, the horizontal axis means the number of selected light source positions and the vertical axis means the measurability of each reflection component. Figure 9(a) and (b) show the ratio of the measurability of the diffuse and the specular reflection component, respectively. In Figure 9(b), when the number of selected light source position is 1, the ratio of measurability of the specular reflection component is 0%. This is because at least 2 different light source positions are needed to determine the specular reflectance and the surface roughness parameter. With respect to the diffuse reflectance parameter, when the number of selected light source positions is 5, the ratio of the measurability of the diffuse reflection component is 100%. As for the specular reflectance and the surface roughness parameters, even when the object is measured with all possible positions, the ratio of the measurability of the specular reflection component is 83.53%. In our method, the ratio of measurability of the specular reflection component is 83.46% with automatically selected 12 light source positions. Since the ratio of measurability of both reflection component is comparable to that using all possible light source positions, the experiment shows that the proposed method is much valid.

Figure 10 shows rendered images using the estimated parameters in Figure 8 with five different virtual light sources. The origin of the coordinate system locates at the object's barycenter, the positive direction of x, y and z axes

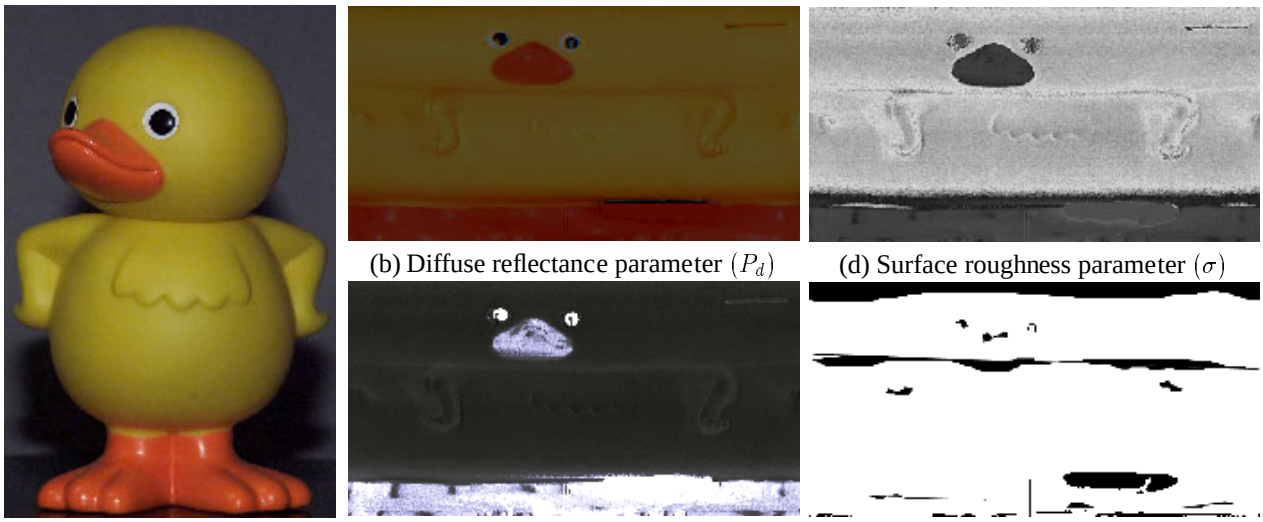

(a) Object (b) Diffuse reflectance parameter (P_d) (c) Specular reflectance parameter (P_s) (d) Surface roughness parameter (σ) (e) Area of observed specular reflection

Figure 8. A measured object and estimated reflectance parameters.

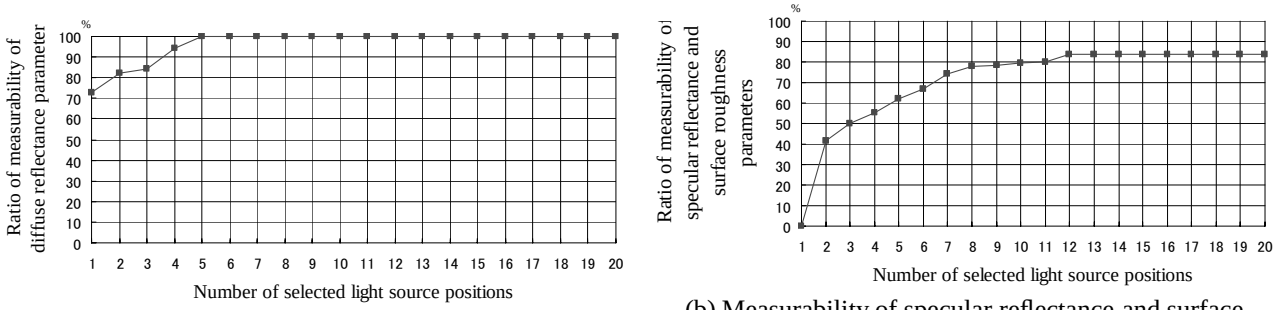

(a) Measurability of diffuse reflectance parameter

(b) Measurability of specular reflectance and surface roughness parameters

Figure 9. The possibility of estimating reflectance parameters with respect to the number of light positions.

agree with the right, upper and forward directions on the image plane, respectively. The viewing position locates at (0.0, 0.0, 20.0) and the viewing direction is toward negative direction of z axis. The virtual light source rotates around y axis. The direction of the virtual light is captioned by the degree of rotation in (a)∼(e). Let 0 degree be the front of the object. The width, height and depth of the object are approximately 18.6 cm, 25.0 cm, and 14.8 cm, respectively. Note that the diffuse reflectance parameter represents the object's texture and the highlight is observed sharply at the doll's leg and beak under each illumination condition.

Nevertheless, since the interreflection is not considered in the present work, parameters for doll's neck are not correctly estimated, where the observed intensity consists of secondary reflection from some object part. Moreover, because some part in the range image is blank with measuring by the laser rangefinder, the object is not rendered well.

4 Conclusions

In this paper, we have proposed a new method of densely estimating non-uniform reflectance properties for almost the whole object surface by using the laser rangefinder. In our approach, multiple light source positions around the laser rangefinder are automatically selected, so that two reflection components are observed densely. The experiments have shown that the proposed method is useful for estimating the reflectance parameters of objects which exhibit non-uniform surface reflectance. However since modeling a light includes some errors and

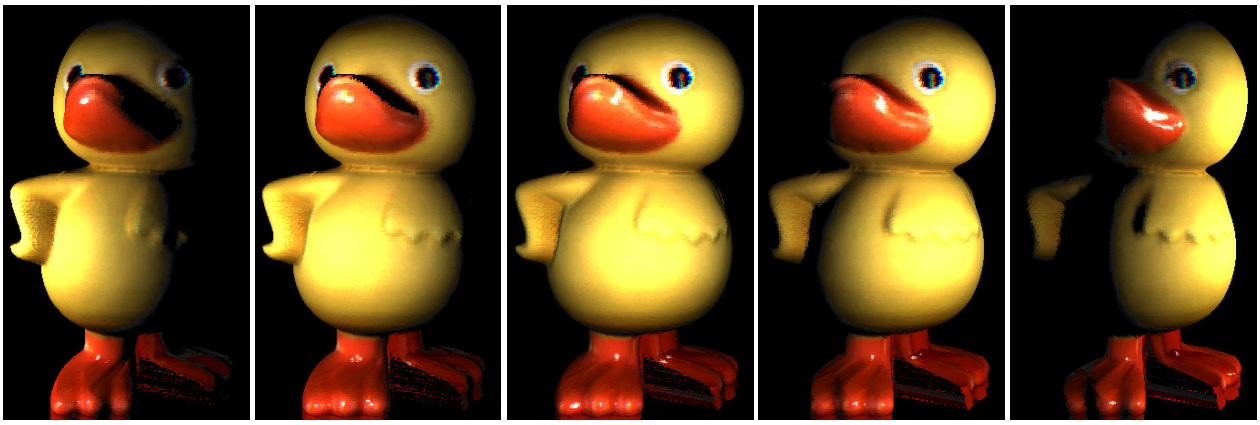

(a) light 1 (-45.0 °) (b) light 2 (-22.5 °) (c) light 3 (0.0 °) (d) light 4 (22.5 °) (e) light 5 (45.0 °)

Figure 10. Rendering of object with virtual light sources.

interreflections are not considered, reflectance parameters are not estimated stably in some part. In the future, we will improve the method so that a light is modeled accurately. We will also investigate a method to consider interreflections all over the object surface.

References

[1] R. Baribeau, M. Rioux, and G. Godin. Color reflectance modeling using a polychromatic laser sensor. *IEEE Trans. on Pattern Anal. Mach. Intell.*, 14(2):263–269, 1992.

[2] J. Foley, A. van Dam, S. Feiner, and J. Hughes. *Computer Graphics Principles and Practice*. Addison-Wesley Publishing Company, 2nd edition, 1993.

[3] K. Ikeuchi and K. Sato. Determining reflectance properties of an object using range and brightness images. *IEEE Trans. on Pattern Anal. Mach. Intell.*, 13(11):1139–1153, 1991.

[4] G. Kay and T. Caelli. Inverting an illumination model from range and intensity maps. *CVGIP: Image Understanding*, 59:183–201, 1994.

[5] S. Lin and S. W. Lee. Estimation of diffuse and specular appearance. *Proc. Int. Conf. on Computer Vision*, 2:855–860, 1999.

[6] S. Lin and S. W. Lee. A representation of specular appearance. *Proc. Int. Conf. on Computer Vision*, 2:849–854, 1999.

[7] J. Lu and J. Little. Reflectance function estimation and shape recovery from image sequence of a rotating object. *Proc. Int. Conf. on Computer Vision*, pages 80–86, June 1995.

[8] Y. Sato, M. D. Wheeler, and K. Ikeuchi. Object shape and reflectance modeling from observation. *Proc. SIGGRAPH '97*, pages 379–387, 1997.

[9] K. E. Torrance and E. M. Sparrow. Theory for off-specular reflection from roughened surfaces. *Journal of Optical Society of America*, pages 1105–1114, 1967.

[10] N. Yokoya and M. D. Levine. Range image segmentation based on differential geometry: A hybrid approach. *IEEE Trans. Pattern Anal. Mach. Intell.*, 11(6):643–649, June 1989.